

On the Formation of N₃H₃ Isomers in Irradiated Ammonia Bearing Ices: Triazene (H₂NNNH) or Triimide (HNHNNH)

Marko Förstel,^[a, d] Yetsedaw A. Tsegaw,^[b] Pavlo Maksyutenko,^[a, d] Alexander M. Mebel,^[c] Wolfram Sander,^[b] and Ralf I. Kaiser^{*[a, d]}

The remarkable versatility of triazenes in synthesis, polymer chemistry and pharmacology has led to numerous experimental and theoretical studies. Surprisingly, only very little is known about the most fundamental triazene: the parent molecule with the chemical formula N₃H₃. Here we observe molecular, isolated N₃H₃ in the gas phase after it sublimates from energetically processed ammonia and nitrogen films. Combining

theoretical studies with our novel detection scheme of photoionization-driven reflectron time-of-flight mass spectroscopy we can obtain information on the isomers of triazene formed in the films. Using isotopically labeled starting material, we can additionally gain insight in the formation pathways of the isomers of N₃H₃ under investigation and identify the isomers formed as triazene (H₂NNNH) and possibly triimide (HNHNNH).

1. Introduction

During the last decades, triazenes—a class of organic molecules carrying the =N–N=N– moiety—have received substantial attention both from the theoretical and organic chemistry communities.^[1] Derived from *cis*- and *trans*-triazene (HN=NNH₂; Scheme 1), the substituted counterparts have significant applications in synthetic chemistry,^[1a, c] polymer science,^[1d] and pharmacology as antitumor drugs such as Dacarbazine, Temozolomide, and Mitozolomide^[2] with their biological activity attributed to their purported capability to alkylate deoxyribonucleic acid (DNA).^[3] Although triazenes have been synthesized for over 65 years, their stem compound^[4] *trans*- and *cis*-triazene (Scheme 1) could not be isolated since triazene undergoes facile acid-catalyzed decomposition.^[5] An unknown isomer of N₃H₃ has been detected mass spectrometrically via signal at mass-to-charge *m/z* = 45 as a transient species by discharging hydrazine (N₂H₄); the ionization energy of the unknown isomer was reported to be 9.6 ± 0.1 eV.^[5a] Triazene (N₃H₃) with a half-

life time of at least 1 ms was also inferred as an intermediate in the radiolysis of an aqueous solution of hydrazine based on a single absorption feature at 230 nm.^[6] The cyclic isomer of triazene, cyclotriazene, was first reported crystallographically in zeolite A, where it was stabilized by a silver cation as Ag(N₃H₃)⁺.^[7] Finally, lithium-ion-complexed species Li(N₃H₃)⁺ of unknown structures were generated in a microwave discharge of hydrazine–helium mixtures.^[8]

The aforementioned spurious indication of “triazene” isomers (N₃H₃) triggered significant computational efforts spanning three decades.^[9] An early study by Nguyen et al. identified a *cis*- and *trans* isomer of triazene (HN=NNH₂) with all six atoms arranged in the same plane (C_s symmetry); the *trans* isomer is thermodynamically more stable by 27 to 38 kJ mol⁻¹ compared to the *cis* structure (Scheme 1).^[9b, c] A later study by Magers et al. identified two additional isomers of triazene, triimide (azimine) and cyclo-triazene (triaziridine) with triimide about 54 to 130 kJ mol⁻¹ and cyclo-triazene about 170 to 190 kJ mol⁻¹ less stable than *trans*-triazene. Therein it was pointed out that triazene is “not exactly planar” and that “low-temperature isolation of these species would likely succeed”.^[9d] These findings were refined by Pye et al.^[9a] 1-amino-1,1-diazene was first located on the potential energy surface by Salter et al.,^[9e] who suggested that this isomer (called isotriazene in their paper) is 42 to 50 kJ mol⁻¹ lower in energy than cyclo-triazene. Combined, these results show that the stabilities of triazenes decrease in the order *trans*-triazene, *cis*-triazene, triimide, 1-amino-1,1-diazene and cyclo-triazene (Scheme 1).

Here, we exploit a novel experimental approach to synthesize N₃H₃ in low-temperature matrices via an interaction of ionizing radiation with frozen films containing ammonia (NH₃) and nitrogen (N₂) along with their deuterated (ND₃) and ¹⁵N-labeled (¹⁵N₂) counterparts. Upon sublimation of the newly formed molecules, N₃H₃ is identified for the first time via fragment-free single-photon vacuum ultraviolet (VUV) photoionization cou-

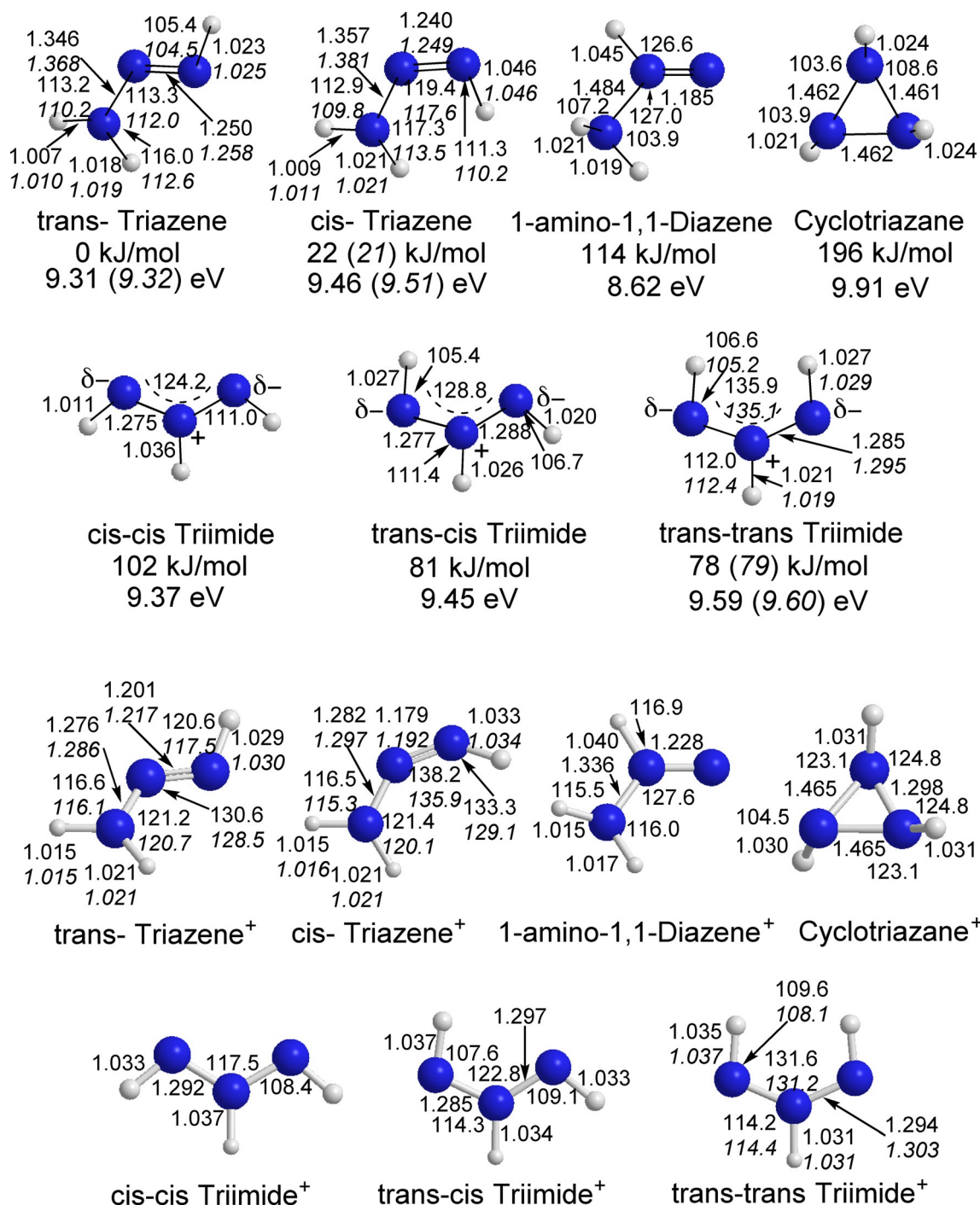
[a] Dr. M. Förstel, Dr. P. Maksyutenko, Prof. Dr. R. I. Kaiser
Department of Chemistry
University of Hawaii, 2545 McCarthy Mall
96822 Honolulu HI (USA)
E-mail: ralfk@hawaii.edu

[b] Y. A. Tsegaw, Prof. Dr. W. Sander
Lehrstuhl für Organische Chemie II
Ruhr Universität Bochum
44780 Bochum (Germany)

[c] Prof. Dr. A. M. Mebel
Department of Chemistry and Biochemistry
Florida International University
11200 SW 8th Street, Miami, FL 33199 (USA)

[d] Dr. M. Förstel, Dr. P. Maksyutenko, Prof. Dr. R. I. Kaiser
W. M. Keck Research Laboratory in Astrochemistry
University of Hawaii, 2545 McCarthy Mall
96822 Honolulu HI (USA)

Supporting Information and the ORCID identification number(s) for the author(s) of this article can be found under <http://dx.doi.org/10.1002/cphc.201600414>.



Scheme 1. Structures, ionization energies, and relative energies with respect to the most stable isomer of the triazene. Distances are given in Ångstrom, angles in degrees. Plain and *italic* numbers are calculated at the B3LYP/6-311G** and CCSD(T)/6-311G** levels of theory, respectively. Ionization energies are adiabatic values. Numbers in parenthesis in *italics* denote values derived with CCSD(T)/6-311G** optimized geometries. The two bottom rows show the structures of the ionic species used for the calculation of the adiabatic ionization energy.

pled to a reflectron time-of-flight mass spectrometer (PI-ReTOF-MS)^[10] through its parent ion at mass-to-charge $m/z = 45$. This observation is substantiated by the detection of its isotopically labeled counterparts N_3D_3 ($m/z = 48$) along with $^{15}NN_2H_3$ ($m/z = 46$), $^{15}N_2NH_3$ ($m/z = 47$), and $^{15}N_3H_3$ ($m/z = 48$), respectively.

Experimental Section

Ice layers with thicknesses of 600 ± 50 nm were prepared from four different gases along with their mixtures. These ices were ammonia (NH_3), D3-ammonia (ND_3), ammonia and nitrogen (NH_3 , N_2 , 1:1.0 \pm 0.2) and ammonia and 15N-nitrogen (NH_3 , $^{15}N_2$, 1:1 \pm 0.2) with purities as follows: NH_3 (Matheson; 99.999%), ND_3 (Isotopes Inc; 99+ % D), N_2 (Matheson; 99.9999%) and $^{15}N_2$ (Cambridge Isotope

Inc. 98 + % ¹⁵N). The gases and/or their mixtures were introduced into the main chamber via a glass capillary array and condensed onto a 5.5 ± 0.2 K cold, rhodium-coated silver wafer. The deposition of each gas took about ten minutes. During the deposition, the pressure in the main vacuum chamber increased from (5 ± 2) × 10⁻¹¹ torr to (3 ± 1) × 10⁻⁸ torr. The ice thickness was monitored during the deposition via in situ He–Ne laser interferometry.^[11] Using Equation (1), a laser wavelength of λ = 632.8 nm and refractive indices of NH₃ and N₂ of 1.35 ± 0.05^[12] and 1.2 ± 0.1^[13] and an angle of incidence of θ = 4°, the number of observed interference fringes (N_f) can be related to the thickness (d) of the ice:

$$(1) \quad d = \frac{N_f \lambda}{2\sqrt{n^2 - \sin^2 \theta}} \quad (1)$$

The composition of the ice mixtures was determined by relating the NH₃ absorption features at 1092 cm⁻¹ with a value of 1.7 × 10⁻¹⁷ cm^[14] to the ice thickness determined by interferometry. Each sample was then irradiated for 60 min with 5 keV electrons at a current of 15 ± 2 nA by scanning the electron beam over the target surface of 0.9 ± 0.1 cm² at an angle of 70° with respect to the surface normal of the substrate. The average deposited dose D per irradiated molecule can be calculated using Equation (2):

$$(2) \quad D = \frac{I t m}{e N_A \rho A} (E_{\text{init}} - f_{\text{trans}} E_{\text{trans}} - f_{\text{bs}} E_{\text{bs}}) \quad (2)$$

where I, t, m, e, N_A, ρ, A and E_{init} are the irradiation current, irradiation time, molecular mass of the molecule, the electron charge, Avogadro's constant, the density of the ice, the irradiated area of the ice, and the initial kinetic energy of the electrons, respectively. The values f_{trans}, f_{bs}, E_{bs}, E_{trans} and I denote the fraction of electrons transmitted through the ice, the fraction of electrons which are backscattered, the average kinetic energy of the backscattered electrons, the average kinetic energy of the transmitted electrons, and the average penetration depth of the electrons, respectively. These values are determined exploiting the Monte Carlo simulation program CASINO^[15] averaging over 20000 trajectories. The deposited energy per ammonia molecule in these experiments is 1.5 ± 0.2 eV. In the mixed ices we determined a dose of 1.3 ± 0.2 eV per irradiated ammonia molecule and 1.9 ± 0.2 eV per irradiated nitrogen molecule. The simulation parameters are summarized in Table 1. After the irradiation, each ice was kept at 5.5 K for one hour. During the irradiation and the equilibration phase, infrared spectra (FTIR, Nicolet6700) were recorded from 6000 to 500 cm⁻¹ with a resolution of 4 cm⁻¹. The substrate was then warmed up with a rate of 0.5 K min⁻¹ to 300 K.

Molecules subliming into the gas phase were photoionized at 10.49 eV, 9.67 eV and 9.1 eV and detected using a reflectron time-of-flight mass spectrometer (ReTOF).^[16] The 10.49 eV photons were generated by frequency tripling of the third harmonic of an Nd:YAG (354.7 nm) (Spectra Physics, PRO-250, 30 Hz) laser in a jet of pulsed xenon (Xe) gas.^[17] 9.67 eV and 9.1 eV photons were produced using resonant four-wave difference mixing of two frequencies (2ω₁ – ω₂).^[18] 9.67 eV photons were generated from two beams overlapping in krypton gas, where the first beam was generated using the frequency-tripled (202 nm) output of a dye laser (606 nm, Rhodamine 610, Sirah, Cobra-Stretch) which was pumped by the second harmonic of an Nd:YAG laser (532 nm). The second laser beam was generated using the direct output of a dye laser (478 nm, Coumarin 480, Sirah, Precision Scan). This dye laser was pumped with the third harmonic of an Nd:YAG laser (355 nm). 9.1 eV photons were via mixing in xenon gas. The first beam was

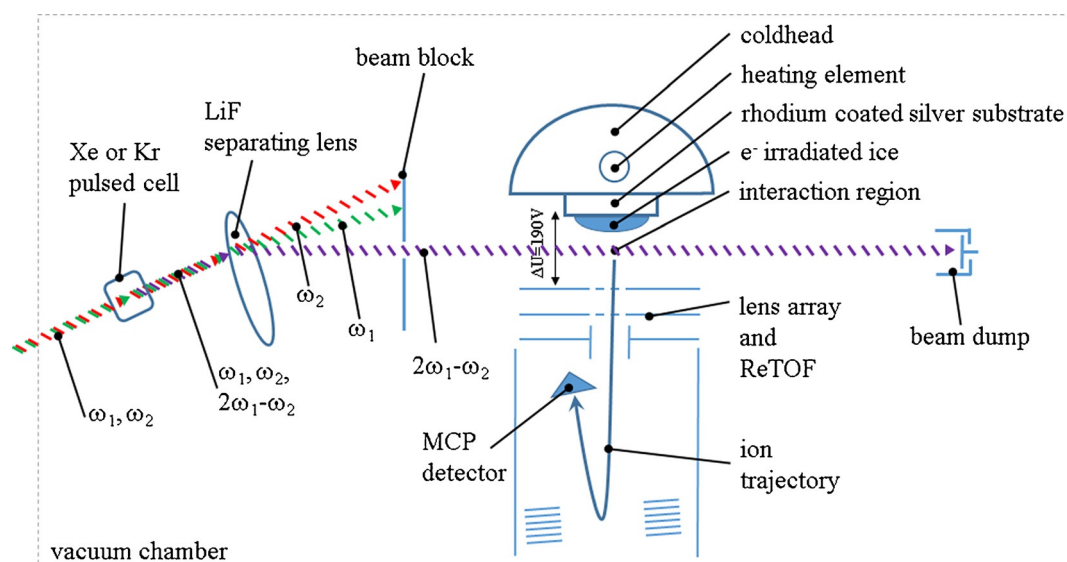
Table 1. Data applied to calculate the irradiation dose per molecule: * marks values from CASINO simulations.

initial kinetic energy of the electrons, E _{init}	5 keV
irradiation current, I	15 ± 2 nA
total number of electrons	(3.4 ± 0.3) × 10 ¹⁴
average kinetic energy of backscattered electrons, E _{bs} * (NH ₃ ice)	3.3 ± 0.9 keV
average kinetic energy of backscattered electrons, E _{bs} * (NH ₃ :N ₂)ice)	3.3 ± 0.9 keV
fraction of backscattered electrons, f _{bs} * (NH ₃ ice)	0.34 ± 0.1
fraction of backscattered electrons, f _{bs} * (NH ₃ :N ₂ ice)	0.35 ± 0.1
average kinetic energy of transmitted electrons, E _{trans} * (NH ₃ ice)	1.5 ± 0.5 keV
average kinetic energy of transmitted electrons, E _{trans} * (NH ₃ :N ₂ ice)	1.6 ± 0.5 keV
fraction of transmitted electrons, f _{trans} * (NH ₃ ice)	0.16 ± 0.05
fraction of transmitted electrons, f _{trans} * (NH ₃ :N ₂ ice)	0.08 ± 0.05
average penetration depth, l* (NH ₃ ice)	365 ± 80 nm
average penetration depth, l* (NH ₃ :N ₂ ice)	350 ± 80 nm
density of the NH ₃ ice, ρ	0.66 ± 0.05 g cm ⁻³
density of the NH ₃ :N ₂ ice, ρ	0.75 ± 0.08 g cm ⁻³
irradiated area, A	0.9 ± 0.1 cm ²
total number of molecules processed	(7 ± 3) × 10 ¹⁷
dose per NH ₃ molecule, D (NH ₃ ice)	1.5 ± 0.4 eV
dose per NH ₃ molecule, D (NH ₃ :N ₂ ice)	1.3 ± 0.4 eV
dose per N ₂ molecule, D (NH ₃ :N ₂ ice)	1.9 ± 0.5 eV

generated using the frequency doubled (222.6 nm) output of a dye laser (445.1 nm, Coumarin 450, Sirah, Cobra-Stretch) which was pumped by the third harmonic of an Nd:YAG laser (355 nm). The second laser beam was generated using the direct output of a dye laser (607 nm, Rhodamine 610, Sirah, Precision Scan). This dye laser was pumped with the second harmonic of an Nd:YAG laser (532 nm). The respective laser beams were then coupled using a dichroic mirror and led into a differentially pumped vacuum chamber through a magnesium fluoride (MgF₂) window. A fused silica bi-convex lens (Thorlabs LB4265, f = 150 mm) focused the respective beams into a section of a pulsed jet of krypton (9.67 eV) or xenon (9.1 eV) released by a piezoelectric pulsed valve operated at 30 Hz. A lithium fluoride (LiF) lens mounted off-center from the beam path of the generated and fundamental laser beams separated the beams according to their refractive indices spatially. A pin hole behind this lens was then used to block the fundamentals (ω₁; ω₂) from entering the interaction region, and only the desired light was introduced into the main chamber. A schematic of the experimental setup is shown in Scheme 2.

Computational Methods

Calculated structures, ionization energies and relative energies with respect to the lowest-energy isomer of N₃H₃ are shown in Scheme 1. Geometries of various N₃H₃ isomers and transition states as well as of products of N₃H₃ dissociation were optimized at the hybrid density functional B3LYP level of theory^[19] with the 6–311G** basis set^[20] and vibrational frequencies were computed using the same B3LYP/6–311G** method to characterize stationary points as local minima or transition states and to obtain zero-point energy corrections (ZPE). For selected isomers and their cations we additionally performed geometry optimization at the coupled clusters CCSD(T) level of theory^[21] with the same 6–311G** basis set. Single-point energies at the optimized geometries were then refined employing the explicitly correlated coupled clusters CCSD(T)-F12 method^[22] with Dunning's correlation-consistent cc-pVTZ-f12



Scheme 2. Schematic top view of the experimental setup. Subliming molecules are ionized by VUV light generated via four-wave mixing and detected in a reflectron time-of-flight mass spectrometer (not to scale).

basis set,^[23] the CCSD(T)-F12/cc-pVTZ-f12 energy is expected to closely approach the complete basis set frozen core fc-CCSD(T)/CBS limit and hence the relative energies from the present calculations are anticipated to provide accuracy within 5 kJ mol^{-1} or better. Vertical and adiabatic ionization energies for all N_3H_3 isomers were evaluated at the same CCSD(T)-F12/cc-pVTZ-f12/B3LYP/6-311G** + ZPE(B3LYP/6-311G**) level and also calculated were appearance energies of fragmentation pathways. The CCSD(T) and CCSD(T)-F12 energies were computed within the restricted closed (open) shell scheme with restricted HF wavefunction used as a reference, RHF-RCCSD(T). All electronic structure calculations were carried out using the Gaussian 09^[24] and MOLPRO 2010^[25] program packages. The potential energy diagram including N_3H_3 isomers, transition states, and dissociation products is illustrated in Figure 1. Energy calculations are summarized in Table S1. Geometric structures of all isomers and transition states are summarized in Table S2. Calculated vibrational frequencies are summarized in Table S3. Vertical and adiabatic ionization energies are presented in Table S4. The transition states in these tables are labeled according to Figure 1.

2. Theoretical Results

Our computations identified seven N_3H_3 isomers. In agreement with earlier theoretical calculations, *trans*- (*trans*- H_2NNNH) and *cis*-triazene (*cis*- H_2NNNH) are the most stable isomers of N_3H_3 with the *trans* isomer residing 21 kJ mol^{-1} below the *cis* structure. Both are connected via a transition state lying 187 kJ mol^{-1} higher in energy than *trans*- H_2NNNH . The next group of isomers in the order of stability includes triimides (HNHNH), which can exist as *trans-trans*, *trans-cis*, and *cis-cis*; 78 , 81 , and 102 kJ mol^{-1} above *trans*- H_2NNNH , respectively. The different triimides are connected to one another via rotational barriers around the N–N bonds ranging between 107 and 132 kJ mol^{-1} . The nitrene (H_2NNHN) and cyclic isomer (*c*- N_3H_3) are the least stable isomers being 120 and 178 kJ mol^{-1} higher in energy than *trans*-triazene. It should be noted that

we performed CCSD(T)/6-311G** geometry optimization for selected most favorable N_3H_3 isomers, *trans*- and *cis*- H_2NNNH and *trans-trans*-HNHNH, and their cations. The differences between optimized B3LYP and CCSD(T) geometric parameters (Scheme 1) appeared to be rather minor and did not exceed 0.03 \AA and 4° and in most cases were much lower than these maximal values. The effect of the use of the CCSD(T)/6-311G** optimized geometries on the relative energies of the N_3H_3 isomers obtained by single-point CCSD(T)-F12 calculations were below 1 kJ mol^{-1} . For adiabatic ionization energies, the differences between the values obtained with B3LYP and CCSD(T) geometries were only 0.01 eV for *trans*- H_2NNNH and *trans-trans*-HNHNH and 0.05 eV for *cis*- H_2NNNH .

Triimides can be formed from triazenes by 1,2-H migrations from the terminal NH_2 group to the central nitrogen atom overcoming barriers of 265 kJ mol^{-1} (*trans*- $\text{H}_2\text{NNNH} \rightarrow \text{trans-cis}$ -HNHNH) and 259 kJ mol^{-1} (*cis*- $\text{H}_2\text{NNNH} \rightarrow \text{trans-trans}$ -HNHNH). Alternatively, a 1,2-H shift from the terminal NH moiety to the central nitrogen leads from *trans*- H_2NNNH to H_2NNHN via a 299 kJ mol^{-1} barrier. The latter can ring-close to *c*- N_3H_3 , overcoming a significant barrier of 272 kJ mol^{-1} . An alternative pathway is the decomposition to molecular nitrogen plus ammonia via a lower barrier of only 81 kJ mol^{-1} . The cyclic *c*- N_3H_3 isomer can also be formed by ring closure in *trans-cis*-HNHNH going through a barrier of 238 kJ mol^{-1} . The thermodynamically most favorable dissociation channel of *trans*-triazene is *trans*- $\text{H}_2\text{NNNH} \rightarrow \text{H}_2\text{NNHN} \rightarrow \text{N}_2 + \text{NH}_3$, leading to the products exoergic by 193 kJ mol^{-1} but the highest barrier on this pathway is at 299 kJ mol^{-1} . *Trans*-triazene can also directly lose molecular hydrogen (H_2) producing hydrogen azide (HN_3) with an endoergicity of 62 kJ mol^{-1} and overcoming a barrier of 304 kJ mol^{-1} . Both *trans*- and *cis* conformations of triazene can dissociate to amidogen (NH_2) plus dinitrogen monohydride (N_2H) by a cleavage of the N–N single bond without an exit barrier. The products lie 199 kJ mol^{-1} higher in energy than

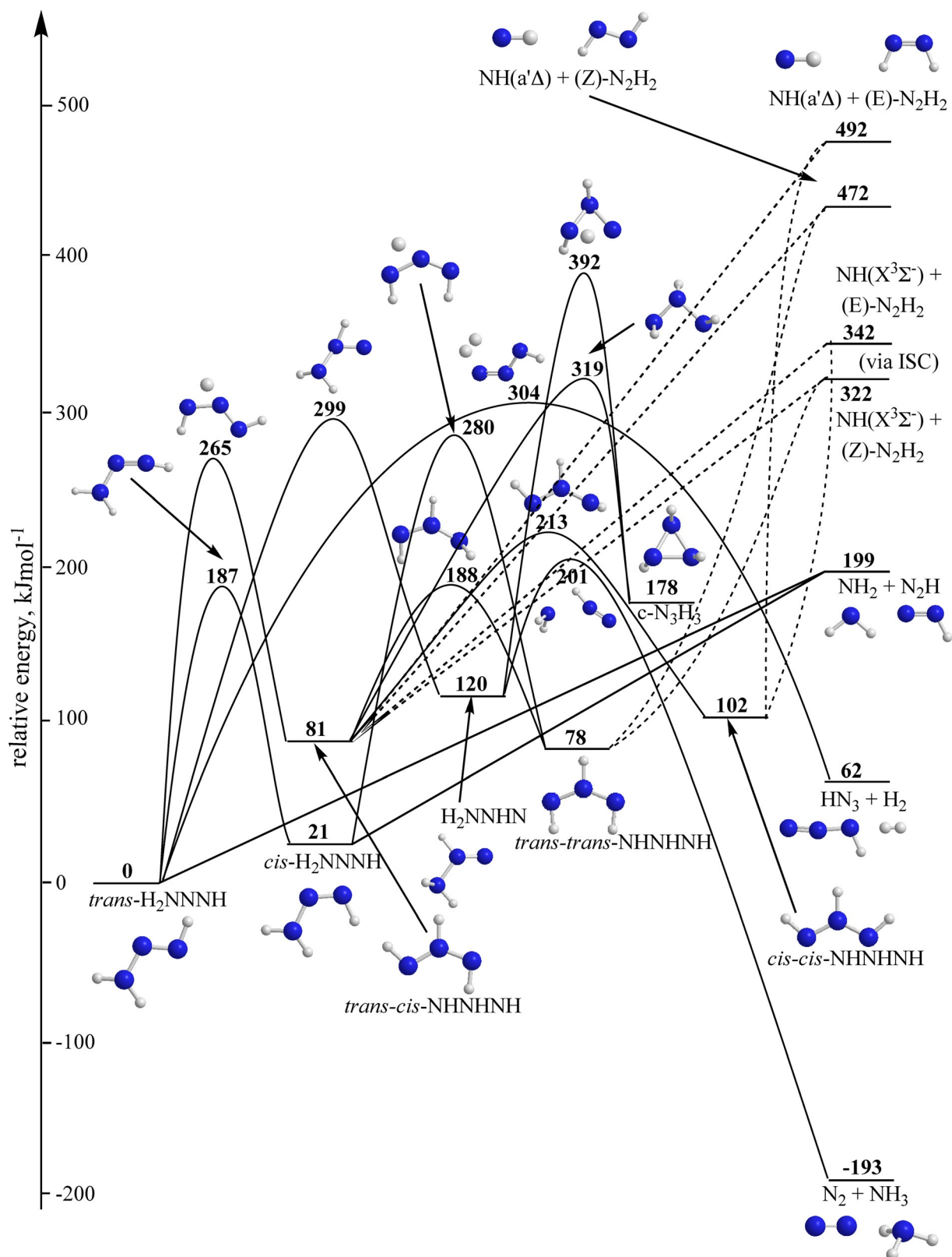


Figure 1. Singlet potential energy surface (PES) of possible N_3H_3 isomers together with predicted decomposition pathways. Dashed lines indicate spin-forbidden decomposition pathways resulting in the formation of triplet ground state imidogen ($NH; X^3\Sigma^-$) and towards the lowest-lying singlet state ($NH; a^1\Delta$).

trans- H_2NNNH . Finally, various triimides can in principle decompose to ground triplet state imidogen ($NH; X^3\Sigma^-$) plus diimide

(*Z*)/(*E*- N_2H_2), 322 and 342 kJ mol^{-1} above *trans*-triazene. The triplet ground state of imidogen ($NH; X^3\Sigma^-$) lies 150 kJ mol^{-1} [26]

below the first excited state singlet state (the spin allowed product), and a decay involving a N–N bond rupture is likely to proceed via singlet–triplet intersystem crossing (ISC). Both possibilities are shown in Figure 1.

3. Experimental Results

The PI-ReTOF-MS results are shown in Figure 2 and Figure 3, which include the data of irradiated ammonia measured at three different ionization energies (left) and, measured all at an ionization energy of 10.49 eV, the PI-ReTOF-MS data of irradiated ND₃, NH₃:N₂ and NH₃:¹⁵N₂ ice (right). Dominating all spectra measured with 10.49 eV is the signal at mass-to-charge ratio of 17 from the host matrix molecule ammonia (NH₃) and, respectively at $m/z=20$ from ND₃. This signal depicts a sublimation onset of 75 ± 2 K, peaks at around 105 ± 2 K and reaches zero intensity above $130 \text{ K} \pm 5$ K. A second TPD peak is observed at this m/z ratio between 150 K and 190 K, with a maximum at around 175 K. The next strongest contribution is observed at a mass-to-charge ratio of $m/z=32$, which is observable at all three ionization energies. This TPD peak is observed in the 145 to 200 K range, peaking at around 155 K. The experiment at

10.49 eV with the isotopically labeled compounds show a peak with the same TPD profile at mass-to-charge ratios of $m/z=36$ (ND₃ ice) and at $m/z=34, 35$ and 36 with intensity decreasing in that order in the NH₃:¹⁵N₂ ice. The next highest contribution is found in the 10.49 eV probed NH₃ ice at a mass-to-charge ratio of $m/z=45$. This TPD profile is observed in the 150 to 190 K region with a peak at around 175 K. This profile is also observed in the 9.67 eV experiment but not in the 9.1 eV experiment. The ND₃ experiment reveals a peak with similar shape at a mass-to-charge ratio of $m/z=48$, but reduced in intensity by a factor of six compared to the ammonia ice. The NH₃:N₂ experiment also exposes this feature, but with an intensity reduced by a factor of 2.5 compared to the ammonia experiment. The NH₃:¹⁵N₂ experiment depicts intensity with a similar TPD profile at mass-to-charge ratios of $m/z=45, 46$ and 47 (Figure 2 f and Figure 3 f). Again, the intensity decreases as the mass-to-charge ratio rises with factors of 0.24, 0.12 and 0.06 compared to the peak at $m/z=45$ from the pure NH₃ ice. At a mass-to-charge ratio of $m/z=30$ we also observe a TPD profile in the range from 157 to 180 K, peaking at 172 K. This peak is observed in the pure ammonia ice only in the 10.49 eV experiment, where it reveals a peak intensity comparable to that

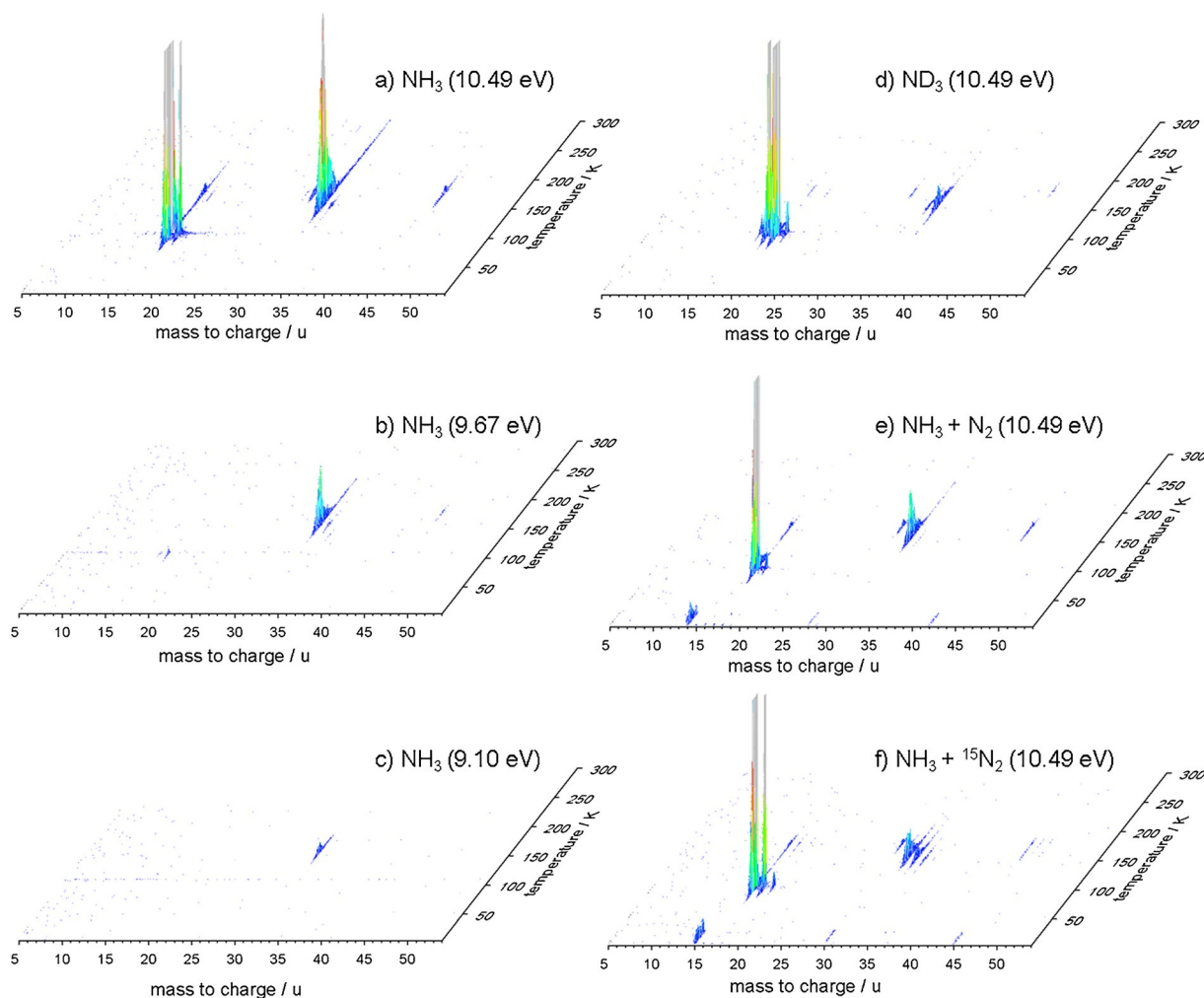


Figure 2. PI-ReTOF-MS spectra with the initial ice composition and the ionization energy given in each panel.

of the TPD profile at a mass-to-charge ratio of $m/z=45$ (Figure 2a and Figure 3a). In the $\text{NH}_3:\text{N}_2$ ice mixture, this peak is a factor of two higher in intensity than that of $m/z=45$ (Figure 2e and Figure 3e). We also observe a very small signal at a mass-to-charge ratio of $m/z=29$ in the ammonia ice at 10.49 eV (Figure 2a and Figure 3a). The TPD profile of this signal shows some intensity in the same range as that of $m/z=45$. However, the signal-to-noise ratio of that signal is very poor. No signal is observed at a mass-to-charge ratio of $m/z=28$.

4. Discussion

Due to the simplicity of the host ice, consisting only of two different atoms, the molecular identification of the observed mass-to-charge ratios is straightforward. The signal at $m/z=30$ must stem from a molecule with the chemical formula N_2H_2 ,

$m/z=32$ from N_2H_4 and $m/z=45$ from N_3H_3 . Molecular nitrogen (N_2) is not observed because its ionization energy (IE = 15.58 eV^[26]) resides well above our highest ionization energy of 10.49 eV. The N_2H_2 isomer was identified as *cis*- and/or *trans*-diimide ($m/z=30$, IE = 9.58 eV).^[27] The N_2H_4 isomer is hydrazine ($m/z=32$, IE = 8.1 eV). With this low ionization energy it is the only molecule observed in the 9.1 eV experiment. In order to identify the isomers of N_3H_3 we have to use data obtained at different ionization energies. Figure 3a depicts the TPD profile of all subliming molecules with $m/z=45$ and an ionization energy below 10.49 eV. Sublimation starts at 150 K and the intensity increases slowly up to a temperature of 173 K. After that we observe a further sharp increase in intensity, which reaches its maximum at 180 K. At 185 K the intensity is back to 20% of its maximum value and then slowly decreases towards zero at around 200 K.

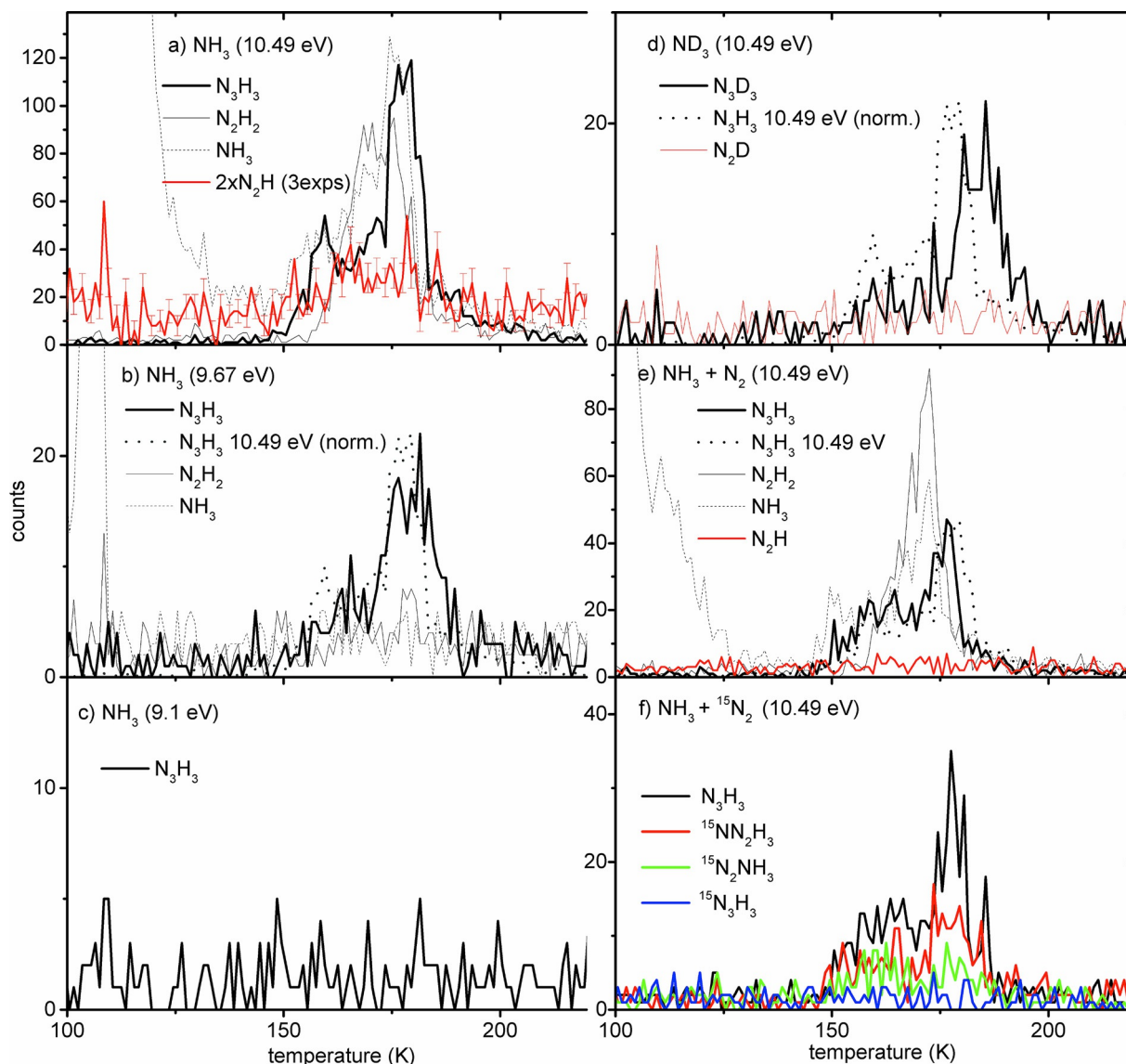
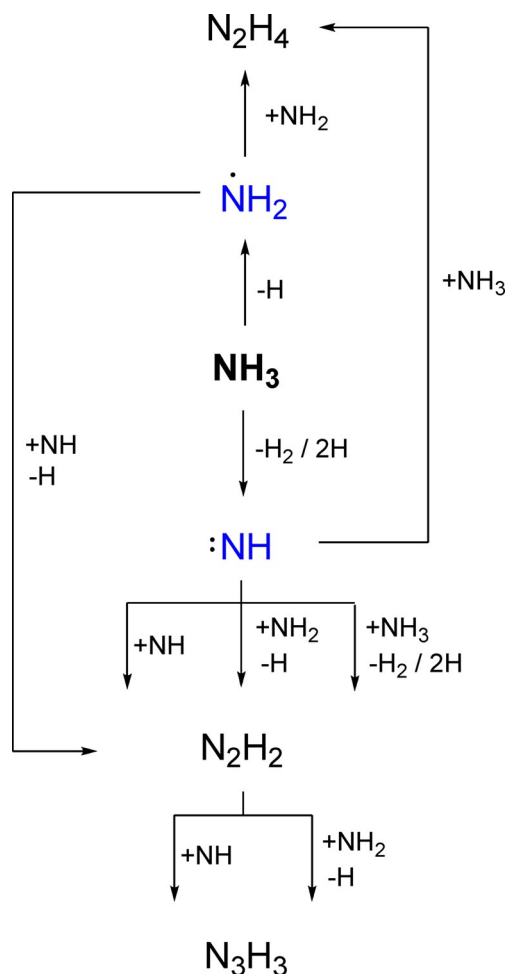


Figure 3. TPD profiles extracted from the PI-ReTOF-MS spectra shown in Figure 2. For intensity and shape comparison, the TPD trace of NH_3 ice at 10.49 eV (a) is included normalized to the respective spectrum as a dotted line in (b), (d) and (e).

Figure 3b shows the result when the subliming molecules are probed using an ionization energy of 9.67 eV. It can be seen that the total observed intensity is a factor of six lower than that measured in the 10.49 eV experiment. The TPD profile, however, shows the same shape as that measured at 10.49 eV. For comparison, the normalized 10.49 eV TPD profile is shown in Figure 3b as a dotted line. Decreasing the ionization energy further we arrive at Figure 3c. Here, at 9.1 eV ionization energy, we observe no signal at this mass-to-charge ratio at all. Comparing these observations with the calculated ionization energies we can already conclude that neither iso-triazene nor cyclo-triazene are detected. Iso-triazene can be excluded because the ionization energy in the 9.1 eV experiment is well above the ionization energy of iso-triazene ($IE = 8.62$ eV). The fact that the shape of the TPD profile remains unchanged when changing the ionization below that of cyclo-triazene (Figure 3b) is a very strong indication that cyclo-triazene is not observed in our experiment.

A discrimination between the remaining isomers, triazene and triimide, based solely on their ionization energies is complicated because of the small differences in their ionization energies and the uncertainty of the calculated ionization energies in the order of up to ± 0.2 eV.^[28] However, there is one observation that suggests that the observed isomers are *cis*- and/or *trans*-triazene, but not triimide. That is, we observe a small signal at a mass-to-charge ratio of $m/z = 29$, which has a TPD profile that matches that of the trace at $m/z = 45$. The appearance energy of the N_2H^+ fragment from *trans*-triazene is 10.26 eV and from *cis*-triazene it is 10.03 eV. This suggests that signal at $m/z = 29$ can only stem from fragmented *cis*- and/or *trans*-triazene. It cannot originate from triimide because our computations suggest that this isomer cannot fragment to $N_2H^+ + NH_2$ upon ionization at 10.49 eV. It needs to be noted that the observed intensity is barely above the noise level and that even if it were higher, it would not exclude that triimide is formed. However, it does imply that at least some of the observed signal stems from *cis*- and/or *trans*-triazene. Another argument why the observed isomer could be *trans*-triazene is the fact that only hydrogen tunneling is necessary to arrive from any of the triimides or the *cis*-triazene to the energetically lowest lying *trans*-triazene. Processes like this were shown to have half-life times of two hours at temperatures as low as 11 K and a barrier of 126 kJ mol^{-1} .^[29] We reach the sublimation temperature of around 170 K 6 h 40 min after irradiation stopped and the calculated barriers are in the same order of magnitude as in the systems discussed in Ref. [29] (Figure 1).

After having established that mostly triazene and also possibly triimide are forming in the ice, let us now concentrate on the potential formation pathways of these molecules. We suggest that the most likely formation pathway towards N_3H_3 occurs via the diimide (N_2H_2) intermediate after reaction with either imidogen via $N_2H_2 + :NH \rightarrow N_3H_3$ or with amidogen via $N_2H_2 + \cdot NH_2 \rightarrow N_3H_3 + H$ as shown in the last step in Scheme 3. Both, imidogen and amidogen, are primary formation products of the irradiation process. Besides the computationally predicted decomposition pathways and energetics, the four following experimental observations strongly suggest that diimide (N_2H_2)



Scheme 3. Principal reaction pathways towards the formation of N_3H_3 starting with NH_3 and with N_2H_2 as an intermediate. The primary irradiation products are shown in blue. Also included are two principal reaction pathways towards N_2H_4 .

and not the main final irradiation product hydrazine (N_2H_4) or other intermediates like HN_3 or HN_2 are intermediates in the N_3H_3 formation. They also show that a formation of N_3H_3 involving molecular nitrogen (N_2) is unlikely.

First, the N_3H_3 yield decreases by a factor of 2.5 when comparing the NH_3 to the $NH_3:N_2$ ices. The yield of N_2H_2 decreases by a factor of 1.6 in these ices. These values are only in agreement with each other if we assume that N_2H_2 is a precursor in N_3H_3 formation. This first point is further backed by the observation that the ratio of diimide molecules with no ^{15}N atoms to diimide molecules with one ^{15}N atom is, with 0.53 ± 0.05 , the same as that of N_3H_3 to $^{15}NN_2H_3$ (0.52 ± 0.05).

Second, using the same argument we can exclude hydrazine (N_2H_4) as a precursor because the yield of N_2H_4 decreases by a factor of 4.3 when comparing its yields in the NH_3 and the $NH_3:N_2$ ice. This means that if N_2H_4 were a precursor in N_3H_3 production, the N_3H_3 yield should decrease at least as much as the N_2H_4 yield.

Third, in the $NH_3:N_2$ ices, we observe a decrease in the yield of N_3H_3 compared to pure ammonia ice of about 2.5. The shape of the TPD curve is, however, unchanged. This indicates

that the same isomers are forming in both systems. The isotopically labeled ices reveal the reason for the strong decrease in N_3H_3 yield: even though the $^{15}N_2$ part of the ice contributes two thirds of all the nitrogen atoms available in the ice, $56 \pm 3\%$ of the observed triazene molecules did not incorporate any ^{15}N atom. $29 \pm 2\%$ of the molecules built in only one ^{15}N , and merely $14 \pm 2\%$ hold two ^{15}N atoms. A possible reaction pathway leading to triazene including isotopically labelled molecular nitrogen without initial N_2 cleavage would be $^{15}N_2 + H \rightarrow \cdot^{15}N_2H$ followed by $\cdot^{15}N_2H + \cdot NH_2 \rightarrow ^{15}N_2NH_3$. Only 14% of the observed N_3H_3 molecules have that signature despite the abundance of ^{15}N atoms. This means that hypothetical formations of N_3H_3 via N_2H (from $N_2 + H$) or via N_3H (from $N_2 + NH$) are not important pathways.

Fourth, the remaining possibility to form N_3H_3 starts with a cleavage of molecular nitrogen (N_2) to two nitrogen atoms, which could then form imidogen ($:NH$) after recombination with a hydrogen atom; imidogen can react with diimide (N_2H_2) to N_3H_3 . Also these pathways can only play a minor role in the formation of N_3H_3 since they would result in $^{15}NN_2H_3$. All these experimental considerations together with our energetic calculations are pointing to N_2H_2 as the reaction intermediate in the N_3H_3 formation.

As depicted in the reaction scheme (Scheme 3), there are two possibilities to arrive from N_2H_2 to N_3H_3 . Using our technique we cannot differentiate between these two. The same holds for the formation of N_2H_2 . Here, four different formation pathways are feasible. One starting with the primary irradiation product $\cdot NH_2$ and three possibilities starting with the primary irradiation product $:NH$.

5. Conclusions

We have processed homogeneous ammonia (NH_3) and deuterated ammonia (ND_3) films as well as mixed $NH_3 : N_2$ and $NH_3 : ^{15}N_2$ films with energetic electrons at low temperatures to study the formation of the hitherto poorly described N_3H_3 isomers. N_3H_3 as well as its isotopically labeled counterparts N_3D_3 , $^{15}N_3H_3$, $^{15}N_2H_3$ and $^{15}NN_2H_3$ are observed via their mass-to-charge ratios $m/z = 45, 48, 48, 47$ and 46 , respectively, after they are photoionized upon sublimation. Using our newly established method of photoionization driven reflectron time-of-flight mass spectroscopy (PI-ReTOF-MS), a sensitive detection scheme utilizing tunable photon energies, in combination with the calculation of ionization energies of the possible N_3H_3 isomers, we show that the observed N_3H_3 signal can only stem from the triazene and/or the triimide isomers. Both the iso-triazene and the previously described cyclo-triazene are not observed. Further, by calculating the appearance energy of the fragment ions of triazene and triimide and comparing those to our experimental observations we present evidence that at least parts of the observed N_3H_3 signal must originate from *trans*- and/or *cis*-triazene. To elucidate the formation mechanism of N_3H_3 we have then conducted isotopic substitution studies and suggest that the N_3H_3 formation occurs preferably with the diimide (N_2H_2) as a precursor via the reaction with imidogen (NH). These considerations are backed by energetic cal-

culations of the possible decomposition pathways of N_3H_3 . Summarizing we can conclude that our study gives a detailed insight in the formation of N_3H_3 in energetically processed films and hope that it helps in future attempts to isolate molecular triazene to make it available as a direct component in the synthesis of more complex molecules.

Acknowledgements

The authors thank the W. M. Keck Foundation and the U. S. Army Research Office (W911NF-14-1-0167) for support. M.F. acknowledges funding from the DFG (FO 941/1). The Bochum team (YAT, WS) thanks the Cluster of Excellence RESOLV (EXC 1069), funded by the Deutsche Forschungsgemeinschaft, for support.

Keywords: ammonia · matrix isolation · nitrogen chain molecules · triazene · triimides

- [1] a) D. B. Kimball, M. M. Haley, *Angew. Chem. Int. Ed.* **2002**, *41*, 3338–3351; *Angew. Chem.* **2002**, *114*, 3484–3498; b) A. Schmiedekamp, R. H. Smith, Jr., C. J. Michejda, *J. Org. Chem.* **1988**, *53*, 3433–3436; c) M. L. Gross, D. H. Blank, W. M. Welch, *J. Org. Chem.* **1993**, *58*, 2104–2109; d) J. Stebani, O. Nuyken, T. Lippert, A. Wokaun, *Die Makromolekulare Chemie, Rapid Commun.* **1993**, *14*, 365–369; e) F. Marchesi, M. Turriziani, G. Tortorelli, G. Avvisati, F. Torino, L. De Vecchis, *Pharmacol. Res.* **2007**, *56*, 275–287; f) *Triazanes: Chemical, Biological and Clinical Aspects*, Springer Science + Business Media, LLC, **1989**; g) Y. A. Jeilani, T. M. Orlando, A. Pope, C. Pirim, M. T. Nguyen, *RSC Adv.* **2014**, *4*, 32375–32382.
- [2] a) D. E. V. Wilman, *The Chemistry of Antitumor Agents*, Glasgow, Blackie; New York: Chapman and Hall, **1990**; b) E. L. Carvalho, A. P. Francisco, J. Iley, E. Rosa, *Bioorg. Med. Chem.* **2000**, *8*, 1719–1725; c) M. Ludwig, M. Kabičková, *Collection of Czechoslovak Chemical Communications* **1996**, *61*, 355–363.
- [3] R. B. Livingston, *Single Agents in Cancer Chemotherapy*, Springer Science & Business Media, **2012**.
- [4] K. Saunders, *Practical Organic Chemistry*, 2nd ed., Longmans, Green and Co., New York, **1949**, pp. 157–179.
- [5] a) S. Foner, R. L. Hudson, *J. Chem. Phys.* **1958**, *29*, 442–443; b) S. Foner, R. Hudson, *Adv. Chem. Ser.* **1962**, *36*, 34.
- [6] a) E. Hayon, M. Simic, *J. Am. Chem. Soc.* **1972**, *94*, 42–47; b) J. W. Sutherland, *J. Phys. Chem.* **1979**, *83*, 789–795.
- [7] a) Y. Kim, J. W. Gilje, K. Seff, *J. Am. Chem. Soc.* **1977**, *99*, 7057–7059; b) N. H. Heo, Y. Kim, J. J. Kim, K. Seff, *J. Phys. Chem. C* **2016**, *120*, 5277–5287.
- [8] T. Fujii, C. P. Selvin, M. Sablier, K. Iwase, *J. Phys. Chem. A* **2002**, *106*, 3102–3105.
- [9] a) C. C. Pye, K. Vaughan, J. F. Glistler, *Can. J. Chem.* **2002**, *80*, 447–454; b) M. T. Nguyen, L. Hoesch, *Helv. Chim. Acta* **1986**, *69*, 1627–1637; c) M. T. Nguyen, J. Kaneti, L. Hoesch, E. S. Dreiding, *Helv. Chim. Acta* **1984**, *67*, 1918–1929; d) D. H. Magers, A. A. Salter, R. J. Bartlett, C. Salter, B. A. Hess, Jr., L. J. Schaad, *J. Am. Chem. Soc.* **1988**, *110*, 3435–3446; e) E. A. Salter, R. Z. Hinrichs, C. Salter, *J. Am. Chem. Soc.* **1996**, *118*, 227–228.
- [10] a) S. Maity, R. I. Kaiser, B. M. Jones, *Phys. Chem. Chem. Phys.* **2015**, *17*, 3081–3114; b) R. I. Kaiser, S. Maity, B. M. Jones, *Phys. Chem. Chem. Phys.* **2014**, *16*, 3399–3424.
- [11] a) O. S. Heavens, *Optical Properties of Thin Solid Films*, Butterworths Scientific Publications, London, **1955**; b) M. S. Westley, G. A. Baratta, R. A. Baragiola, *J. Chem. Phys.* **1998**, *108*, 3321–3326.
- [12] M. Á. Satorre, J. Leliwa-Kopystynski, C. Santonja, R. Luna, *Icarus* **2013**, *225*, 703–708.
- [13] M. Á. Satorre, M. Domingo, C. Millán, R. Luna, R. Vilaplana, C. Santonja, *P&SS* **2008**, *56*, 1748–1752.
- [14] L. B. d'Hendecourt, L. J. Allamandola, *Astron. Astrophys. Sup.* **1986**, *64*, 453–467.

- [15] D. Drouin, A. R. Couture, D. Joly, X. Tastet, V. Aimez, R. Gauvin, *Scanning* **2007**, *29*, 92–101.
- [16] a) B. M. Jones, R. I. Kaiser, *J. Phys. Chem. Lett.* **2013**, *4*, 1965–1971; b) M. Förstel, P. Maksyutenko, B. M. Jones, B.-J. Sun, S.-H. Chen, A. H. H. Chang, R. I. Kaiser, *ChemPhysChem* **2015**, *16*, 3139–3142.
- [17] a) S. Maity, R. I. Kaiser, B. M. Jones, *Faraday Discuss.* **2014**, *168*, 485–516; b) S. Maity, R. I. Kaiser, B. M. Jones, *Astrophys. J.* **2014**, *789*, 36.
- [18] a) J. W. Hepburn, *Laser Techniques in Chemistry*, Wiley, New York, NY, **1994**; b) R. Hilbig, R. Wallenstein, *Appl. Opt.* **1982**, *21*, 913–917; c) R. Hilbig, G. Hilber, A. Lago, B. Wolff, R. Wallenstein, *Nonlinear Optics and Applications* **1986**, 613.
- [19] a) A. D. Becke, *J. Chem. Phys.* **1993**, *98*, 5648–5652; b) C. Lee, W. Yang, R. G. Parr, *Phys. Rev. B* **1988**, *37*, 785–789.
- [20] R. Krishnan, M. Frisch, J. Pople, *J. Chem. Phys.* **1980**, *72*, 4244–4245.
- [21] a) G. D. Purvis, R. J. Bartlett, *J. Chem. Phys.* **1982**, *76*, 1910–1918; b) G. E. Scuseria, H. F. Schaefer III, *J. Chem. Phys.* **1989**, *90*, 3700–3703; c) G. E. Scuseria, C. L. Janssen, H. F. Schaefer III, *J. Chem. Phys.* **1988**, *89*, 7382–7387; d) J. A. Pople, M. Head-Gordon, K. Raghavachari, *J. Chem. Phys.* **1987**, *87*, 5968–5975.
- [22] a) G. Knizia, T. B. Adler, H.-J. Werner, *J. Chem. Phys.* **2009**, *130*, 054104; b) T. B. Adler, G. Knizia, H.-J. Werner, *J. Chem. Phys.* **2007**, *127*, 221106–224100.
- [23] K. A. Peterson, T. B. Adler, H.-J. Werner, *J. Chem. Phys.* **2008**, *128*, 084102.
- [24] *Gaussian 09 (Revision D.01)*, M. J. Frisch, G. W. Trucks, H. B. Schlegel, G. E. Scuseria, M. A. Robb, J. R. Cheeseman, G. Scalmani, V. Barone, B. Men-
nucci, G. A. Petersson, H. Nakatsuji, M. Caricato, X. Li, H. P. Hratchian,
A. F. Izmaylov, J. Bloino, G. Zheng, J. L. Sonnenberg, M. Hada, M. Ehara,
K. Toyota, R. Fukuda, J. Hasegawa, M. Ishida, T. Nakajima, Y. Honda, O.
Kitao, H. Nakai, T. Vreven, J. A. Montgomery Jr., J. E. Peralta, F. Ogliaro,
M. Bearpark, J. J. Heyd, E. Brothers, K. N. Kudin, V. N. Staroverov, R. Ko-
bayashi, J. Normand, K. Raghavachari, A. Rendell, J. C. Burant, S. S. Iyen-
gar, J. Tomasi, M. Cossi, N. Rega, J. M. Millam, M. Klene, J. E. Knox, J. B.
Cross, V. Bakken, C. Adamo, J. Jaramillo, R. Gomperts, R. E. Stratmann,
O. Yazyev, A. J. Austin, R. Cammi, C. Pomelli, J. W. Ochterski, R. L. Martin,
K. Morokuma, V. G. Zakrzewski, G. A. Voth, P. Salvador, J. J. Dannenberg,
S. Dapprich, A. D. Daniels, Ö. Farkas, J. B. Foresman, J. V. Ortiz, J. Cio-
slowski, D. J. Fox, Gaussian, Inc., Wallingford, CT, **2013**.
- [25] H.-J. Werner, P. J. Knowles, G. Knizia, F. R. Manby, M. Schutz, GAUSSIAN
09 version 2010.1 ed., **2010**, p. a package of ab initio programs.
- [26] NIST, in *NIST Standard Reference Database Number 69* (Ed.: P. J. Linstrom,
Mallard, W. G.), **2011**.
- [27] M. Förstel, P. Maksyutenko, B. M. Jones, B. J. Sun, A. H. H. Chang, R. I.
Kaiser, *ChemPhysChem* **2015**, *16*, 3139–3142.
- [28] a) R. I. Kaiser, S. P. Krishtal, A. M. Mebel, O. Kostko, M. Ahmed, *Astrophys.
J.* **2012**, *761*, 178; b) O. Kostko, J. Zhou, B. J. Sun, J. S. Lie, A. H. Chang,
R. I. Kaiser, M. Ahmed, *Astrophys. J.* **2010**, *717*, 674.
- [29] a) P. R. Schreiner, H. P. Reisenauer, D. Ley, D. Gerbig, C.-H. Wu, W. D.
Allen, *Science* **2011**, *332*, 1300–1303; b) P. R. Schreiner, H. P. Reisenauer,
F. C. Pickard IV, A. C. Simmonett, W. D. Allen, E. Mátyus, A. G. Császár,
Nature **2008**, *453*, 906–909.

Manuscript received: April 22, 2016
Final Article published: June 27, 2016